AVHRR rectification using orbital navigation and image matching

André R. S. Marçal*, Janete Borges**
Faculdade de Ciências, Universidade do Porto

ABSTRACT

Polar orbital satellites with low spatial resolution sensors, such as the AVHRR, provide global coverage with a short repetition period. The data is directly transmitted to ground stations, and can be distributed immediately after data acquisition. Near real time applications can be implemented if the adequate processing tools are available. One task usually needed is the geometric correction of image data. Automatic methods, based on satellite orbital parameters, can in some cases provide satisfactory results. However, the identification of Ground Control Points (GCPs) is generally required in order to achieve registration errors below the pixel size. A fully automatic method for the geometric registration of AVHRR data is proposed here. The method comprises four stages: (i) an initial image transformation based on orbital parameters, (ii) image segmentation of this image into 3 main classes (land, water, cloud) and 9 additional classes of mixed water and land at various levels, (iii) automatic GCP collection by image matching, (iv) final image production combining both orbital and GCP information. The method was tested on ten images of the Iberian Peninsula, and proved effective in accurately geo-referencing sub-sections of an AVHRR scene of medium dimension in a few minutes.

Keywords: AVHRR, image rectification, geometric corrections, image segmentation, image matching

1. INTRODUCTION

Earth observation satellites acquire enormous amounts of data from the surface and atmosphere of the Earth every day. The data is usually transmitted to ground stations and stored in archives for subsequent processing. A number of sensors, onboard meteorological and environmental satellites, provide frequent global coverage of the Earth with low spatial resolution multi-spectral images. Some satellite stations, such as the Dundee Satellite Receiving Station (www.sat.dundee.ac.uk), provide on-line access to satellite data a few minutes after the data acquisition, allowing for near real time environmental monitoring applications to be implemented. However, as the raw satellite data is usually not satisfactory, a fast chain of processing is required so that the information extracted from the satellite data becomes available in practical time.

1.1 The AVHRR data

The Advanced Very High Resolution Radiometer (AVHRR) onboard National Oceanographic and Atmospheric Administration (NOAA) satellites, provides data of the Earth surface and atmosphere since 1978 [1]. The NOAA series of satellites is an operational program, providing 2 working satellites continuously. Currently the operational satellites are NOAA 16 and NOAA 17, but the data used in this work was obtained from NOAA 14. The AVHRR has a nominal ground resolution of 1.1 km at nadir and a wide swath of 2800 km, which allows for complete Earth coverage every 12 hours [2]. The AVHRR instrument has 5 spectral bands: band 1 on the visible (0.58-0.70μm), band 2 on the near infrared region (0.72-1.00μm), band 3 on the mid-infrared (3.58-3.98 μm), and bands 4 and 5 on the thermal infrared part of the electromagnetic spectrum (10.3-11.3 μm and 11.5-12.5 μm, respectively) [1]. The digital data is collected in 10-bit resolution and transmitted to ground in various modes, including the High Resolution Picture Transmission (HRPT) mode that is used for real-time transmission of the 1 km image data [2]. The AVHRR sensor was initially designed for meteorological and oceanographic purposes, but has been used for many other environmental applications. Some of these applications can benefit from data access in near real time. A number of processing steps are usually needed before the required information can be obtained from the satellite data. These can include image calibration, additional image production, image classification, geometric correction and image registration. Most of these tasks can be automated, with various levels of difficulties.

* amarcal@oa.fc.up.pt; phone: +351 220100873; fax: +351 220100809; www.fc.up.pt; Departamento de Matemática Aplicada, Rua do Campo Alegre, 687, 4169-007 Porto, Portugal; ** janeteborges@gmx.net; phone: +351 220100840

1.2 Existing geometric correction methods for AVHRR images

There are several methods for correcting the geometric distortions present on satellite images. The geometric correction methods can be divided into three groups: (i) modelling the nature and magnitude of the sources of distortion, using these models to establish a correction formulae [3]; (ii) empirical, using Ground Control Points (GCPs) – points identified on the image whose geographic coordinates are known; (iii) mixed, using both methods (i) and (ii). Methods of type (i) are very effective in that they can be automated. However, its precision is constrained on the exact knowledge of the satellite orbit and the sensors attitude. In the case of the AVHRR there are uncertainties of around 0.1 degrees in roll pitch and yaw [4]. The empirical methods can theoretically provide good quality geometrically corrected satellite images. However, this requires that a large number of well spread GCPs are available, as high order transformation functions need to be used. This is an obvious limitation as the identification of GCPs is a time consuming task. Furthermore, the number of places where it is possible to identify GCPs is quite often small due to the characteristics of the study area and to cloud cover. The methods of type (iii) are generally the most effective in that they provide an initial automatic image correction that is further improved by the use of a GCP based transformation. Several methods were developed using a combination of orbital modelling and empirical based corrections for AVHRR images [5,6]. In general, the identification of at least one GCP is required for high accuracy registration to be achieved.

There have been some attempts to fully automate the geometric correction of AVHRR data. Mao et al developed a method based on coastline extraction and matching [7]. Their method is based on a correlation-relaxation technique and is suitable in areas where large cloud free areas of the coastline are available [7]. The method presented here also intends to remove the intervention of an operator, allowing for the registration of the AVHRR image data to be fully automatic.

2. OVERVIEW OF THE METHOD

The method presented here for the geometric correction of AVHRR images involves the four stages listed below.

(i) Initial image transformation (f) of the original AVHRR image, based on orbital parameters, creating a geo-referenced image (*auto*).

(ii) Image segmentation of the *auto* image created into 3 main classes (land, water, and cloud) and an additional 9 classes of various levels of mixed water/land.

(iii) Automatic collection of a set of GCPs, by image matching, that are used to establish a transformation function (g) between the *auto* image and a *reference* image.

(iv) Final image production, directly from the original image, combining both image transformation functions f and g.

These four processing stages are illustrated on Figure 1, for an image of NOAA 14 from the 5th of August 1995. The 500 by 1000 pixel section of the full AVHRR scene used as *raw* image is shown on the top left corner of Figure 1. The geometric distortions are clearly visible on this grey scale representation of AVHRR channel 2 (near infrared).

2.1 Initial image transformation (f)

The initial image transformation is a third order polynomial function, which is obtained using an adapted simplified orbital model [4,5]. This is an automatic task, requiring a number of satellite orbital parameters that are provided with the image data. This geometric correction accounts for distortions due to the Earth curvature and rotation and, to a certain degree, the satellite velocity and sensor orientation. A visual inspection of the *auto* image (top middle of Figure 1) suggests that it is geometrically correct. However, the *auto* image is affected by a low frequency error of several kilometres both in X and Y coordinates, and a high frequency error typically of 1 to 2 km [6]. The reason for this error is that the internal recorded time and the AVHRR attitude are not precisely known

2.2 Automatic establishment of a set of GCPs

A first order polynomial transformation function is generally sufficient to reduce the registration error on the *auto* image to sub pixel level [6]. A set of GCPs is used to establish the transformation function g by the least squares method. An operator could identify the set of GCPs. Instead, this is done automatically using image segmentation and image matching techniques. A *segmented* image (top right of Figure 1) is produced from the *auto* image. The segmentation and image matching tasks will be described in more detail on sections 3 and 4.

2.3 Final image production

The fourth stage is the production of a *final* image. This is done combining the transformation functions f and g (3rd and 1st order polynomial). The final image is produced directly from the raw image by a 3rd order polynomial transformation function, which prevents excessive smoothing due to multiple image resampling

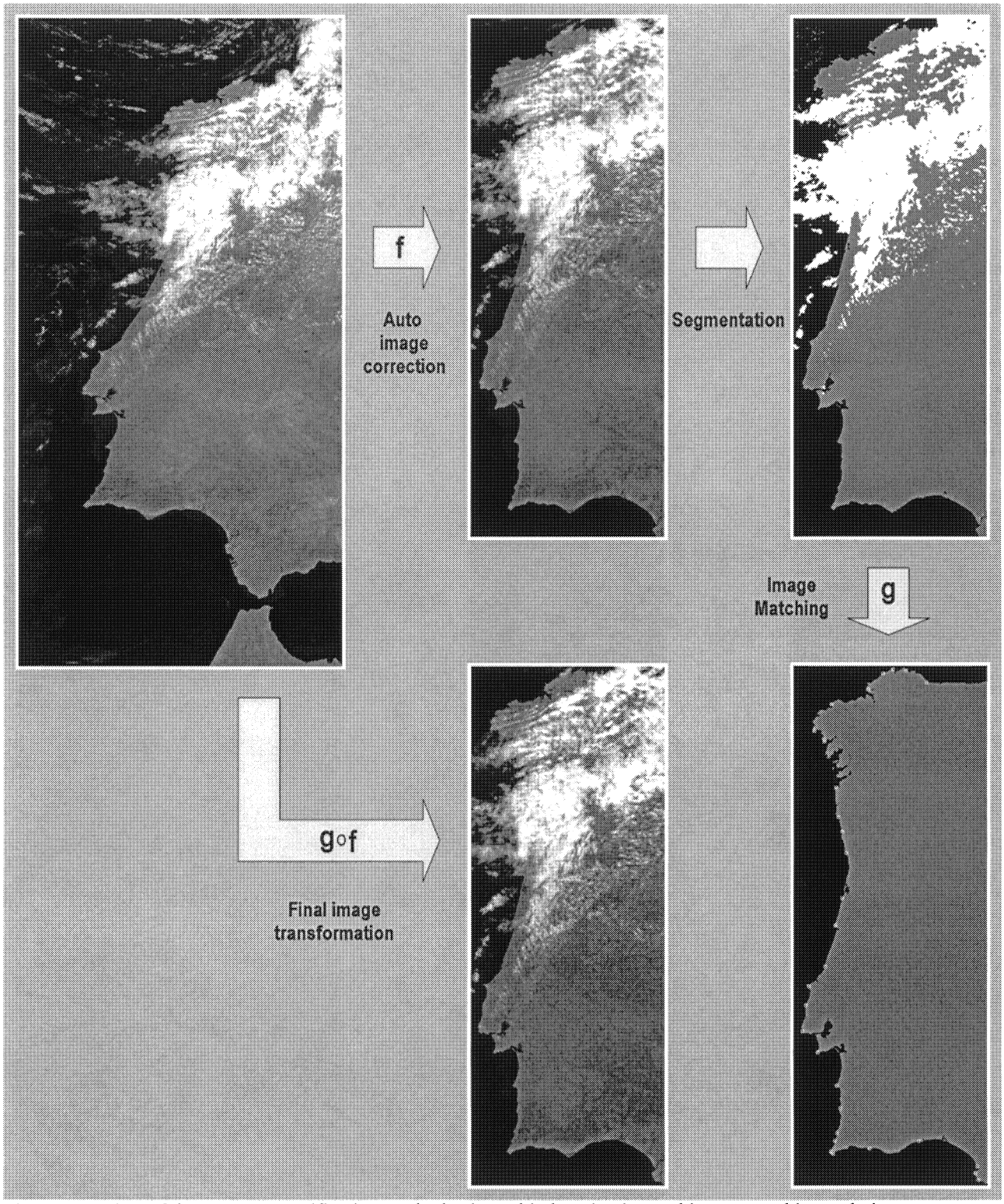

Fig. 1: Overview of the AVHRR rectification method using orbital navigation and image matching techniques.

3. IMAGE SEGMENTATION

The recorded signal of any location varies considerably on images from different days. This is true for all 5 AVHRR bands, as the contribution from the atmosphere is highly variable both temporally and spatially, and strongly influences

the recorded signal. It is therefore not easy to establish a reference image and to apply an image-matching algorithm directly on any of the original image bands. An alternative approach is to segment the AVHRR image into a small number of classes, and then perform the image matching on this segmented version of the AVHRR image. The *auto* image is first classified into pure classes (water, land, cloud) and later refined with additional mixed water/land classes at various proportions.

3.1 Image classification into 'pure' classes

An initial classification is performed on the *auto* image. The classification inputs are radiance calibrated AVHRR bands 1 (RED) and 2 (NIR), and brightness temperature calibrated bands 3 (T3) and 4 (T4). The output is an 8-bit image with the same number of pixels and lines of the input image files. Each pixel is assigned a value 0 (water), 10 (land), 255 (cloudy) or 33 (unclassified). The criteria used for the classification were adapted from existing cloud masking algorithms [8,9]. Pixels with (NIR-RED)>0 are classified as land. Pixels are classified as water if they simultaneously satisfy the following conditions: (NIR-RED)$\leq$0, T4>0, NIR<9, 0.38<NIR/RED<0.89. Pixels that were not classified as land or water will be classified as cloudy if T4<17. Void and noisy pixels are also assigned the value 255. Noisy pixels are rare but void areas occur when the selection of the full AVHRR scene used does not totally cover the area of interest.

3.2 Classification refinement

The results from the initial classification have two flaws: (i) unclassified pixels, (ii) some mixed water/land pixels alongside the coastline are classified as 'purely' water or land. These two flaws are addressed in a second classification process.

A pixel (i,j) is considered a 'contiguous neighbour' to pixel (i',j') if $|i-i'|+|j-j'|=1$. A pixel (i,j) is considered an 'oblique neighbour' to pixel (i',j') if $|i-i'|=1$ and $|j-j'|=1$. Each pixel has 4 'contiguous neighbours' and 4 'oblique neighbours'. The 4 'contiguous' and 4 'oblique' neighbours together form the 3x3 neighbourhood of pixel (i,j).

3.2.1. Unclassified pixels

The pixels that were not classified on the first segmentation process are considered to be 'cloudy' if there is at least one 'cloudy' pixel on its 3x3 neighbourhood. If all 3x3 neighbours of an unclassified pixel belong to one class, then that class is also assigned to the pixel. The mixed water/land algorithm is applied to an unclassified pixel if there are no 'cloudy' pixels on its 3x3 neighbourhood and there is at least one pixel classified as 'land' and one pixel classified as 'water'.

3.2.2. Pixels on the coastline

Each pixel classified as 'pure' land on the first classification process is re-evaluated, taking into account its neighbourhood. If the pixel has at least one 'contiguous neighbour' classified as 'water' then the mixed water/land algorithm is applied to this pixel. This process can maintain the initial classification or change it into one of the mixed water and land classes.

Pure class	Channel 1 Radiance ($Wm^{-2}sr^{-1}\mu m^{-1}$)		Channel 2 Radiance ($Wm^{-2}sr^{-1}\mu m^{-1}$)		Channel 3 Brightness Temperature (°C)		Channel 4 Brightness Temperature (°C)	
	Average	St. Dev	Average	St. Dev	Average	St. Dev	Average	St. Dev
Water	0.389	0.143	0.234	0.169	22.44	3.64	18.32	2.58
Land	1.088	0.415	1.903	0.434	43.67	6.15	38.02	6.59
Cloud	3.759	0.792	4.288	0.880	31.76	4.84	9.80	3.18

Table 1: Typical spectral response of 'pure' classes on the Iberian Peninsula on the summer.

3.2.3. Mixed water/land algorithm

An evaluation of several AVHRR afternoon summer images of the Iberian Peninsula was made, to roughly characterize the spectral response of 'pure' classes. The images were classified using a supervised classification method into water, land and cloud. The average and the standard deviation of each class on channels 1 and 2 (in radiance), and channels 3 and 4 (in brightness temperature) are presented on Table 1.

A pixel selected as a likely candidate for mixed water/land is evaluated according to its radiance on channels 1 and 2 and its brightness temperature on channels 3 and 4. These four values form a 4-dimensional vector. The Euclidian distance of this vector to the average 4-dimensional vector associated to each class, as indicated on Table 1, is

computed. The radiance values are scaled by a factor of 8.8 (channel 1) and 7.4 (channel 2) to allow comparable contributions of the 4 bands to the Euclidian distance. If the smallest distance for a pixel is to the average vector of 'cloud', then the pixel is considered to be 'cloudy'. Otherwise, the pixel is treated as a mixture of water and land. The fraction of land (F_L) is estimated by

$$FL = \frac{1/DL}{1/DL + 1/DW}. \quad (1)$$

where D_L and D_W are the distance between the pixel vector and the average vectors for land and water. The values from equation 1 are multiplied by 10 and rounded, so that each digital number increment corresponds to a 10% increment in F_L. For example, a pixel with 90% water and 10% land is assigned the value 1, one with 80% water and 20% land is assigned the value 2, and so forth. This will result in pixels with less than 5% land being assigned the value 0 (as 'pure' water), and those with 95% or more land being assigned the value 10 (as 'pure' land).

4. IMAGE MATCHING

The *segmented* image produced by the method described on section 3 is used to generate a set of Ground Control Points (GCPs). A reference image and a pre-defined set of Search Points (SPs) are used.

4.1 Reference image

The *reference* image was produced for the area of interest - the west part of the Iberian Peninsula, covering continental Portugal and the Galicia province in northwest Spain. A geo-referenced image file was created using the lat/long coordinate system. The image is 300 by 800 pixels with a pixel size of 1 km^2. A 100 m resolution vector database with coastline and political boundaries [10] was used to estimate the fraction of land and water of each pixel on the *reference* image. The vector database was converted to a raster file covering the same area of the *reference* image but with 100 m pixel. This image was then used to obtain the percentage of land in each 1 km^2 pixel, with the values rounded to increments of 10%. Each pixel on the *reference* image has a value between 0 (water) and 10 (land), with mixed water/land pixels having values between 1 and 9. An overview of the *reference* image is shown on Figure 1 (bottom right), and a detailed view of a section is shown on Figure 2 (centre).

4.2 Search points

A total of 30 SPs were identified on the *reference* image. These were chosen in areas such as capes, peninsulas or other well distinct features alongside the coastline. The location of each SP is marked on the reference image of Figure 1 as a small white square. The location of four SPs on the Southwest of Portugal can be seen on more detail on Figure 2 (left).

4.3 Image matching

A target matrix of 5 by 5 pixels, centred on the first SP, is initially used. A search matrix of 51 by 51 pixels, centred on the same location on the *segmented* image, is selected. If there are pixels contaminated by cloud on the search matrix the SP is rejected. If there are no cloudy pixels the maximum correlation between the search and target sub-matrices is looked for. The correlation (r) between two matrices of the same dimension is given by

$$r = \frac{\sum (g1 - \langle g1 \rangle)(g2 - \langle g2 \rangle)}{\sqrt{\sum (g1 - \langle g1 \rangle)^2 \cdot \sum (g2 - \langle g2 \rangle)^2}}. \quad (2)$$

where g_1 is the target matrix, g_2 the search sub-matrix, and $\langle g_1 \rangle$ and $\langle g_2 \rangle$ are the corresponding arithmetic means of the densities [11]. This equation was implemented for the two dimensional case treated here. The correlation between the target matrix and every sub-matrix of the same size in the search area is computed. In this case, a total of 2209 matches are tested. The centre of the sub-matrix with maximum correlation and the SP coordinates are a first estimate of a GCP. The process is then repeated for the same SP, increasing the target matrix to 7 by 7 pixels. The result will be another estimate for that GCP. The target matrix is further increased to 9 by 9, 11 by 11 and 13 by 13 pixels. A total of 5 estimates for a GCP are now available. The results from the various matching attempts should only diverge by a pixel or so. However, due to similarities in the coastline, it sometimes happens that the best match is not on the correct location. The final X,Y values are obtained as the average of the estimate values that do not lie further than 2 pixels away from the median X,Y estimates. These final X,Y values and the SP coordinates form a GCP.

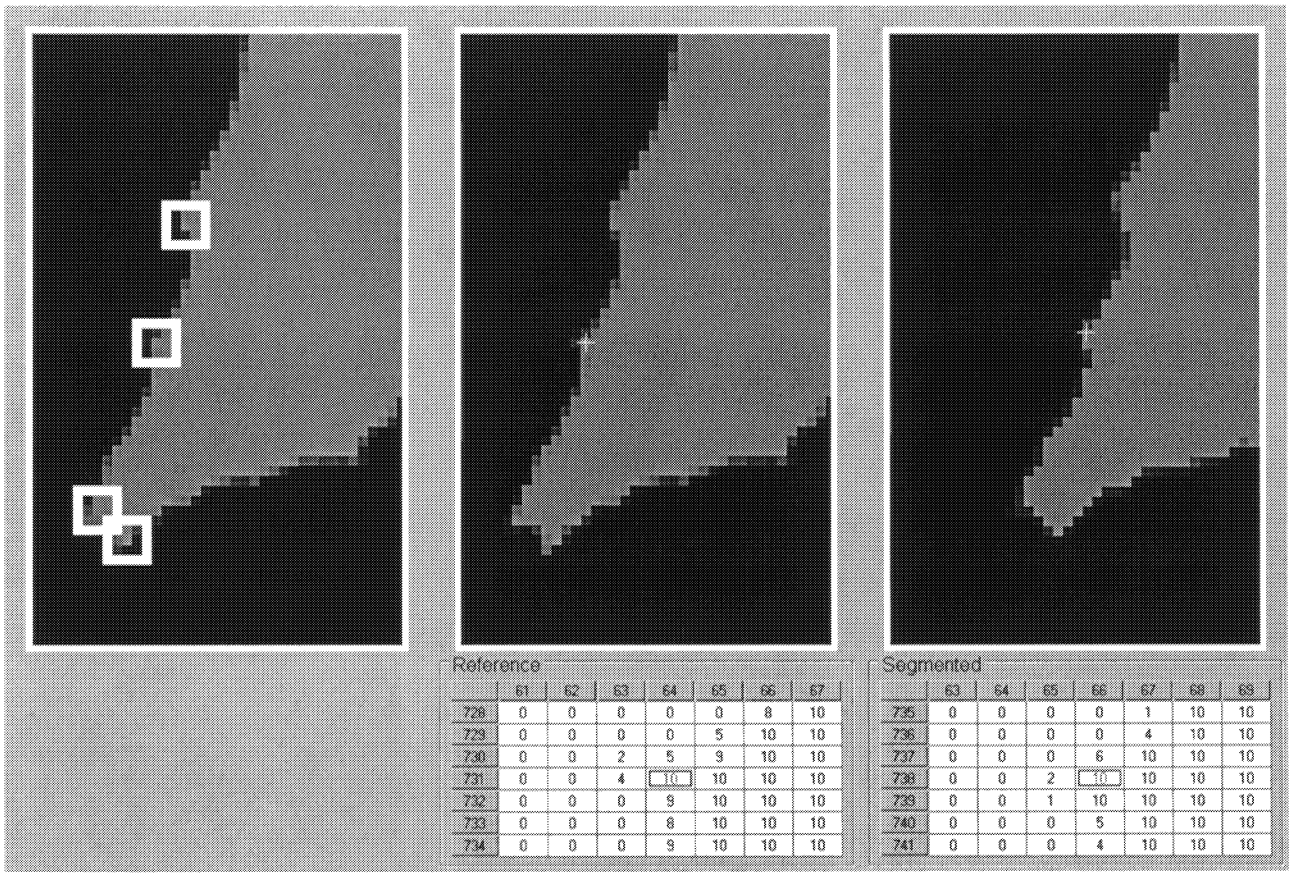

Fig. 2: Detail of the *reference* and *segmented* images around one search point.

To illustrate the process, a SP was selected from an AVHRR image of 5 August 1995. Figure 2 shows a detail of the *reference* image with SPs marked as white squares (left). The numeric values of the reference image around SP 23, with image coordinates (64,731), are also shown on Figure 2 (centre). An inspection of the *segmented* image suggests that the corresponding point should be pixel (66,738). The numeric values of the *segmented* image around this point are also shown on Figure 2 (right). The results of the image matching for this SP are indeed the expected point for all 5 target matrices (Table 2). A GCP is therefore established linking *segmented* coordinates (66,738) and *reference* coordinates (64,731).

	5x5 target matrix	7x7 target matrix	9x9 target matrix	11x11 target matrix	13x13 target matrix
X	66	66	66	66	66
Y	738	738	738	738	738
R	0.9789	0.9767	0.9862	0.9893	0.9892

Table 2: Results of the image matching on one Search Point.

The same matching process is applied to all 30 SPs. The offset on X and Y between the *segmented* and *reference* images is calculated for each GCP. Those GCPs with offset values further away than 3 pixels from the median are rejected. An average offset for *segmented* image is calculated using all valid GCPs. For each SP, a smaller search matrix is now established, centred around the offset corrected coordinates on the *segmented* image. For target matrices of 5x5 and 7x7, search matrices of 11x11 are used. The total area of this search matrix is less than $1/20^{th}$ of the initial size (51x51). The chances of rejecting a SP due to cloud contamination are therefore considerably reduced. A search matrix of 15x15 is used for target matrix of 9x9 and search matrices of 17x17 are used for 11x11 and 13x13 target matrices. The number of GCPs obtained on this second matching process is usually higher, mainly around cloudy areas. The final set of GCPs is used to establish a polynomial transformation function g.

5. RESULTS

The rectification method described was applied on 10 AVHRR images from NOAA 14. The date and overhead time of the images used is listed on Table 3. The average viewing angle was calculated for the area of interest, and is presented on Table 3. Also on Table 3 is the fraction of cloud cover on each image, varying from 0.3% to 32.1%, which were computed from the *segmented* images.

5.1 Rectification results

The final rectified image of 5 August 1995 (AVHRR channel 2) is presented on Figure 3. The full image, 300 by 800 pixels, is displayed (left) with the vector coastline and political boundaries overlaid. A detail of the southwest part is also shown (right) with the 100 m vector data overlaid. A visual inspection of all 10 images tested was carried out. The results were good, with a generally very good agreement from the vector data and the AVHRR rectified images.

The number of valid matches on the first and second process is presented on Table 3. For example, on the image from 5 August 1995, a total of 9 GCPs were obtained on the initial matching and this was increased to 15 GCPs when the search matrices size was reduced. The initial number of GCPs varied from 7 to 18 on the images tested and the final number of GCPs varied from 10 to 25. The number of valid GCPs increased by 4 to 13 from the first to the second matching processes, except for the image from August 19, where there was a decrease from 11 to 10 GCPs. An inspection of the location of each of these GCPs was undertaken. This showed that two of the 11 GCPs identified on the first matching process were wrong. The 10 GCPs on the second matching process were all correct. The correlation coefficient for the polynomial transformation function g was in all cases higher than 0.99.

Image date & time	View angle	% Cloud	No.GCPs (I)	No.GCPs (II)	Pixels tested	$\Delta \leq 2$	$\Delta \leq 5$
5 Aug. 1995, 1409	-21.3	22.6 %	9	15	6509	78.2%	91.6%
6 Aug. 1995, 1359	-12.2	21.8 %	8	15	6909	75.7%	88.3%
7 Aug. 1995, 1348	2.4	6.1 %	11	17	7874	78.4%	91.5%
17 Aug. 1995, 1340	13.0	32.1 %	8	14	4027	74.5%	91.5%
18 Aug. 1995, 1329	25.5	20.8 %	7	11	4663	75.8%	90.0%
19 Aug. 1995, 1318	35.5	9.3 %	11	10	7247	65.1%	77.6%
25 Aug. 1995, 1354	-6.0	2.3 %	12	25	8113	75.3%	90.8%
26 Aug. 1995, 1343	8.3	6.8 %	10	21	7723	80.2%	92.8%
27 Aug. 1995, 1333	22.0	1.0 %	18	24	8213	79.6%	92.5%
28 Aug. 1995, 1317	32.9	0.3 %	18	21	8121	76.9%	90.2%

Table 3: Characteristics of the images tested and summary of results.

5.2 Accuracy evaluation

A test was devised to evaluate the accuracy of the rectification. Using the *reference* image, a bitmap was created using a buffer of 3x3 around the mixed water/land pixels. This bitmap, covering the coastline areas of the *reference* image, has a total of 8251 pixels (36.3% land, 30.1% water and 33.6% mixed water/land). The *final* rectified AVHRR images were segmented, using the same method as the *auto* images. Each unclouded pixel on these images under the test bitmap was compared with the corresponding reference value. The absolute value of this difference (Δ) is an integer between 0 and 10. The number of pixels tested on each images, and the fraction of these pixels with differences up to 2 and up to 5 is presented on Table 3. Except for the image from 19 August, around 75% of the coastline pixels fall in the range $\Delta \leq 2$ and roughly 90% fall in the range $\Delta \leq 5$.

6. CONCLUSIONS

The method proposed proved reasonably effective in the automatic rectification of AVHRR images. As expected, images with high viewing angles tend to suffer from higher registration errors. Most of the high Δ values encountered are on estuaries, which can be justified by the varying conditions on these areas and its effect on the segmentation. The precision of the segmentation is also a source of error. The number of mixed water/land pixels on the *reference* image is generally much higher than on the *segmented* images. This can lead to an error on the automatic identification of GCPs. Another limitation of this method is that only integer pixel values are used in the matching process. The implementation of a sub-pixel matching algorithm is currently underway, and is expected to improve the accuracy of the GCP identification. The characterization of pure classes should be also further explored, to account for different locations and

seasons. Plans for future work also include the use of a digital elevation model for the establishment of the final image transformation. This will improve the registration of high altitude locations.

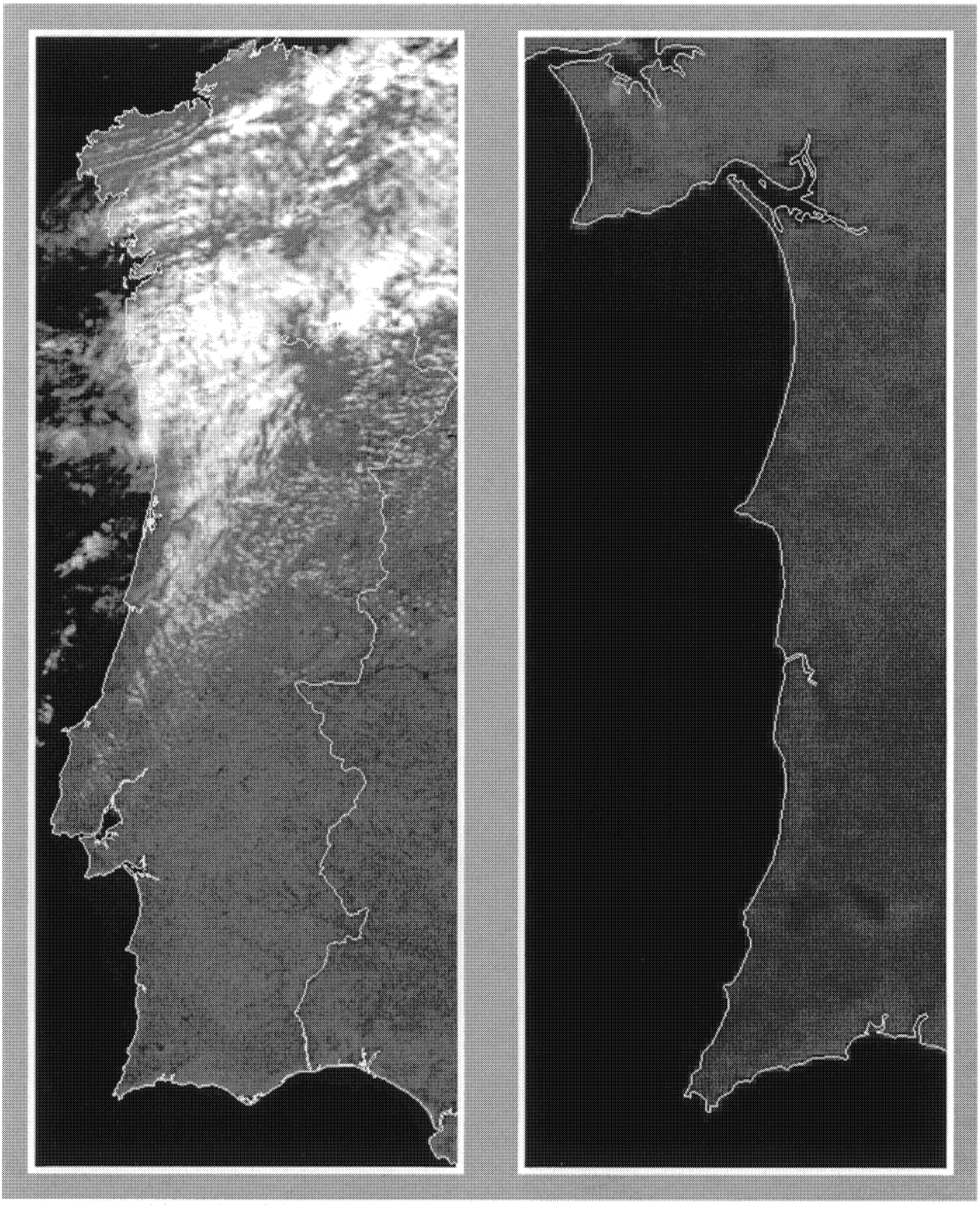

Fig. 3: Example of the final result (5 Aug. 1995) with coastline vector data overlaid; full image (left) and detail (right).

ACKNOWLEDGMENTS

This work was done within the SADAMOS project, financed by the FCT / POCTI. The authors also wish to thank the NERC Dundee Satellite Receiving Station for providing the AVHRR data (www.sat.dundee.ac.uk), and Luís Cardoso for the assistance on establisihing image segmentation criteria.

REFERENCES

1. Kidwell, K.B., *NOAA Polar Orbiter Data Users Guide*, National Oceanic and Atmospheric Administration National Environmental Satellite Data and Information Service, 1995
2. Cracknell, A. P., *The Advanced Very High Resolution Radiometer*, Taylor & Francis, London, 1997
3. Richards, J. A., Xiuping, J., *Remote Sensing Digital Image Analysis*, Springer-Verlag, Berlin and Heidelberg, 1999
4. Brush, R.J.H., "A method for Real-Time Navigation of AVHRR Imagery", *IEEE Transactions on Geoscience and Remote Sensing*, **GE-23**, No. 6, 876-887, 1985
5. Ho, D., Asem, A., "NOAA AVHRR image referencing", *International Journal of Remote Sensing*, **7**, No. 7, 895-904, 1986
6. Marçal, A.R.S., "A new method for high accuracy navigation of NOAA AVHRR imagery", *International Journal of Remote Sensing*, **20**, No. 17, 3273-3280, 1999
7. Mao, Z., Pan, D., Huang, H., Huang, W., "Automatic registration of SeaWiFS and AVHRR imagery", *International Journal of Remote Sensing*, **22**, No. 9, 1725-1735, 2001
8. Muirhead, K., Malkawi, O., "Automatic classification of AVHRR images", *Proceedings of the 4th AVHRR data users' meeting*, 31-34, EUMETSAT, Darmstadt-Eberstadt, Germany, 1989
9. Simpson, J.J., McIntire, T.J., Stitt, J.R., Hufford, G.L., "Improvced cloud detection in AVHRR daytime and night-time scenes over the ocean", *International Journal of Remote Sensing*, **22**, No. 13, 2585-2615, 2001
10. ESRI, 1995, European Countries Data Set, www.esri.com
11. Kraus, K., *Photogrammetry – Fundamentals and Standard Processes*, Dümmler, Bonn, 1993